International Journal on Magnetic Particle Imaging
Vol 3, No 2, Article ID 1706002, 7 Pages

Infinite Science Publishing

Research Article

Preparing system functions for quantitative MPI

Olaf Kosch[a,*] · Ulrich Heinen[b] · James Wells[a] · Lutz Trahms[a] · Frank Wiekhorst[a]

[a]Department 8.2 Biosignals, Physikalisch-Technische Bundesanstalt, Berlin, Germany
[b]Department of Electrical Engineering & Information Technology, University of Applied Sciences Pforzheim, Pforzheim, Germany
*Corresponding author, email: olaf.kosch@ptb.de

Received 28 November 2016; Accepted 13 March 2017; Published online 21 June 2017

Abstract

Magnetic particle imaging (MPI) pledges to provide quantitative information on the spatial distribution of magnetic nanoparticle (MNP). Using a figure-of-eight shaped hosepipe phantom filled with the MPI tracer Ferucarbotran (Resovist precursor), we investigated the quantification capability of a commercial preclinical MPI-scanner (Bruker/Philips Preclinical MPI System, Germany) operated at Charité university hospital, Berlin. For reconstruction of the measured MNP distribution, we used a set of four system functions (SF) acquired with a tracer reference at different iron concentrations (in the range 0.1 mol/L to 1 mol/L). From the analysis of a selected region of interest in the reconstructed images, we found a linear relation between voxel values and the inverse of the concentration of the corresponding reference used in the particular SF acquisition. Based on the precisely known total tracer quantity, we analyzed the MPI image to find the amount of tracer present in each voxel of the phantom. This result was found to be independent of the concentration of the reference sample used in the SF acquisition.

I. Background

Magnetic particle imaging (MPI) is a new tomographic technique for imaging magnetic nanoparticles with great potential for biomedical applications, such as real-time 3D imaging in cardiovascular interventions [1]. MPI detects the magnetic fields generated by the non-linear magnetic susceptibility of superparamagnetic nanoparticles. Recently, two commercial scanner devices for preclinical imaging were installed at Charité university hospital in Berlin and University Medical Center in Hamburg-Eppendorf. In [2] the linearity of the concentration dependent MPI signal intensity was shown within a reconstructed image. The physical principle of MPI theoretically allows a quantitative determination of a tracer distribution, but up to now quantitative information on the particle concentration has only been demonstrated for the x-space MPI [3].

The signals in MPI can be modeled as a linear system of equations, in the frequency domain [4]. As described in [4] the voltage $\boldsymbol{U}(t)$ detected by one receiver coil as a function of time t generated by the dynamic response of MNP at position $\boldsymbol{r}$ in the sample volume V is given by:

$$\boldsymbol{U}(t) = -\mu_0 \frac{\mathrm{d}}{\mathrm{d}t} \int_V \boldsymbol{\sigma}(\boldsymbol{r}) \cdot \boldsymbol{M}(\boldsymbol{r}, t)\, \mathrm{d}V \tag{1}$$

$$= \sum_{n=-\infty}^{\infty} \bar{\boldsymbol{U}}_n \cdot e^{i\frac{2\pi n t}{T}}. \tag{2}$$

Here, $\boldsymbol{\sigma}(\boldsymbol{r})$ denotes the sensitivity of the coil and $\boldsymbol{M}(\boldsymbol{r}, t)$ describes the spatial distribution of the MNP magnetization. By Fourier decomposition we convert to a discrete (voxel) description in the frequency domain, and obtain Eq. (2) with T denoting the scanning time (closed path of the 3D-Lissajous trajectory within the field of view)

and n the number of the complex frequency component. However, some simplifications are implicitly required to obtain a linear equation system: 1) We assume a quasi-stationary spatial distribution of $\boldsymbol{M}$, e.g. the distribution does not change on the time scale of MPI measurement duration (millisecond). 2) The magnetization $\boldsymbol{M}$ linearly scales with concentration; using the number of particles per voxel N/V_{Voxel} this can be written as

$$\boldsymbol{M}_n(r_{\text{Voxel}}) = \frac{\boldsymbol{m}_n(r_{\text{Voxel}})}{V_{\text{Voxel}}} = \frac{N\boldsymbol{\mu}_n(r_{\text{Voxel}})}{V_{\text{Voxel}}}, \tag{3}$$

where the dynamic magnetic moment $\boldsymbol{m}(r_{\text{Voxel}})$ is caused by the N single moments $\boldsymbol{\mu}_n$ of the tracer in a voxel at r_{Voxel}. Thus, if we double the concentration of a tracer in a voxel we double the corresponding voltage measured by the receiver coil.

By introducing the system function (SF) as a complex sensitivity map $\bar{\boldsymbol{S}}$,

$$\bar{\boldsymbol{S}}_n = \boldsymbol{\sigma}(\boldsymbol{r}_{\text{Voxel}}) \cdot \bar{\boldsymbol{\mu}}(\boldsymbol{r}_{\text{Voxel}}, n) \tag{4}$$

we get

$$\bar{\boldsymbol{U}}_n = \int_{\text{FOV}} \bar{\boldsymbol{S}}_n(r_{\text{Voxel}}) \boldsymbol{C}(r_{\text{Voxel}}) \,\mathrm{d}V \tag{5}$$

and in matrix-vector formulation:

$$\bar{\boldsymbol{u}} = \bar{\boldsymbol{S}}\boldsymbol{c}(r_{\text{Voxel}}). \tag{6}$$

The complex system matrix $\bar{\boldsymbol{S}}$ is obtained separately by measurement of the complex voltages $\bar{\boldsymbol{u}}$ of a point-like reference sample of tracer material, which is positioned by a robot at each voxel position r within the FOV. To ensure a high signal-to-noise ratio (SNR), a high tracer concentration of the reference is preferred for this. However, we have to ensure the same dynamic magnetic behavior of the particles in the reference sample and in the subject measurement. In this matter, we have to check even high concentrations of the MNPs [5].

$$\bar{\boldsymbol{S}}(r_{\text{Voxel}}) = \frac{V_{\text{Voxel}}}{c_{\text{ref}} V_{\text{ref}}} \bar{\boldsymbol{u}}(r_{\text{Voxel}}) \tag{7}$$

For quantitative MPI, the values of $\bar{\boldsymbol{S}}$ should be then normalized to the concentration c_{ref} (more precisely, the total amount of MNP) of the employed reference sample. The common description of this normalization shows Eq. (7), including the case if the reference sample volume V_{ref} and the chosen voxel volume V_{Voxel} are different.

Here, we used a hosepipe phantom containing a defined quantity of MPI tracer in a figure-of-eight-shaped distribution. Four different images were reconstructed using the same phantom measurement, but different system functions (SF) acquired at four different tracer concentrations. We looked for the concentration dependency according to Eq. (7) in a selected region of interest, and investigated the possibility of determining absolute values of the iron quantity in each voxel of the image.

II. Materials & Methods

MPI measurements were carried out using the preclinical 3-channel MPI scanner (Bruker/Philips Preclinical MPI System, Germany) operated at Charité university hospital Berlin. The device is a field free point (FFP) scanner moving the FFP on a 3D Lissajous trajectory at three slightly different frequencies (based at the data sampling frequency of 2.5 MHz divided by 102/96/99) at 12 mT amplitude. Additionally, static selection field gradients of $(G_x/G_y/G_z) = (1.25/1.25/2.5)$ T/m are applied. With these parameters, the trajectory covers a field of view (FOV) of $19.2 \times 19.2 \times 9.6\,\text{mm}^3$ in x-, y- and z- direction. For measurements and image reconstructions, we used the supplied scanner software ParaVision 6.0/MPI (Bruker BioSpin, Germany). In the reconstruction, we have used the Kaczmarz's algorithm [6] with 20 iterations and a regularization factor of $\lambda = 10^{-5}$.

II.I. System functions

The measurement-based system functions (SF) are obtained using a cubic reference sample of 8.0 μL volume to give a sufficient SNR for the SFs at lower concentrations. We measured SFs of Ferucarbotran (Meito Sangyo, Japan; Ferucarbotran is the precursor of the MRI liver contrast agent Resovist) at four different iron concentrations: $c_{\text{ref}}(\text{Fe}) = 1$ mol/L (1:1, undiluted), $c_{\text{ref}}(\text{Fe}) = 0.5$ mol/L (1:2 dilution in H2O), $c_{\text{ref}}(\text{Fe}) = 0.2$ mol/L (1:5), and $c_{\text{ref}}(\text{Fe}) = 0.1$ mol/L (1:10). Following the rule of superposition valid for linear systems, we increased the sampling density of the SF based on the size ($2 \times 2 \times 2\,\text{mm}^3$) of the reference sample. This dense sampling of the SF produces a more detailed description, especially at higher harmonics. Fig. 1 compares the SF results at different resolutions for a mixing order of 15. The raw sampling in Fig. 1 a) has shifted the position of the extrema and zero lines. This effect becomes stronger for mixing orders over 15, this is a key consideration as the image reconstruction quality is especially dependent on the higher harmonics [4]. However, the measurement of the SF with $35 \times 35 \times 35$ voxels takes more than 40 h. Hence, we scanned the SF on a grid of 32 by 32 by 16 voxels in x-, y- and z-directions. We applied a geometrical size of $22 \times 22 \times 11\,\text{mm}^3$ for the SF to avoid artifacts at boundaries of the FOV [6]. Every SF recording took 21 h with 100 averages at each voxel position, and was corrected for a slow drift with background measurements after each 16-voxel position (automatically done by the ParaVision software). We kept the number of selected frequency components/equations in the reconstructions constant at 2835. Therefore, we applied four different thresholds, for $c_{\text{ref}}(\text{Fe}) = 1$ mol/L a SNR ≥ 33, for $c_{\text{ref}}(\text{Fe}) = 0.5$ mol/L

10.18416/ijmpi.2017.1706002

a SNR ≥ 13.305, for $c_{\text{ref}}(\text{Fe}) = 0.2$ mol/L a SNR ≥ 5.81, and for $c_{\text{ref}}(\text{Fe}) = 0.1$ mol/L a SNR ≥ 4.

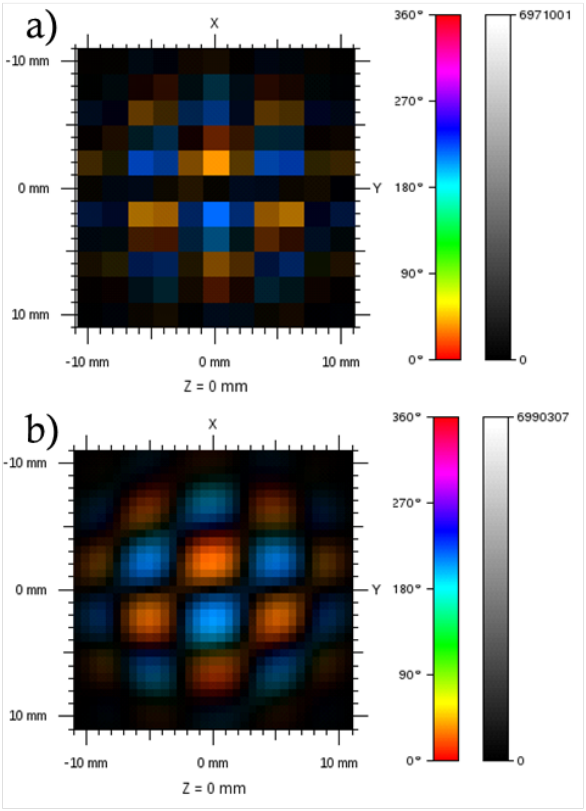

Figure 1: Representation of the x-y-plane in the SF of Ferucarbotran ($c_{\text{ref}}(\text{Fe}) = 1$ mol/L) for the mode $= 5f_x + 7f_y + 3f_z$, in a sampling of a) $11 \times 11 \times 11$ and b) $35 \times 35 \times 35$ voxels using SFView [7].

II.II. Phantom measurement

We designed a figure-of-eight shaped hosepipe phantom with 1.0 mm inner tube diameter and a distance of approximately 10 mm between the centers of both loops as shown in Fig. 2.

By means of a syringe, a 41.6 μL bolus volume of Ferucarbotran at an iron concentration of $c_{\text{ref}}(\text{Fe}) = 0.2$ mol/L (resulting in a total iron amount of 464.6 μg) was positioned at the "eight loops", while the rest of the tube was kept empty. The measurements were carried out using the same acquisition parameters as for SF measurements, but without averaging.

III. Results

We reconstructed four different MPI images from one phantom measurement (see Sec. II.II) using the four individual SFs recorded at different reference sample concentrations (see Sec. II.I). As shown in Fig. 3, all reconstructions nicely resolve the figure-of-eight like spatial distribution of the tracer. With the inner pipe diameter of 1 mm, we are at the achievable resolution limit of the applied selection field. The high voxel density in the SF allows the resolution of the continuous particle track of the phantom in the reconstructed particle distribution. Fig. 4 depicts the x-y-plane (layer 7 of 16) without interpolation for the four reconstructions. Ideally, these images should be identical, since we used the same MPI measurement data for the reconstruction. However, we clearly observe differences in the image quality. Surprisingly, the best contrast occurs in the image using the SF obtained at the lowest concentration ($c_{\text{ref}}(\text{Fe}) = 0.1$ mol/L) (Fig. 3 a)). The values in the SF are related to the concentration of the reference sample used. It seems that the inversion process used during image reconstruction is more sensitive to noise for SFs using higher concentration samples. Applying the normalization of the SF with Eq. (7) should help to avoid this effect.

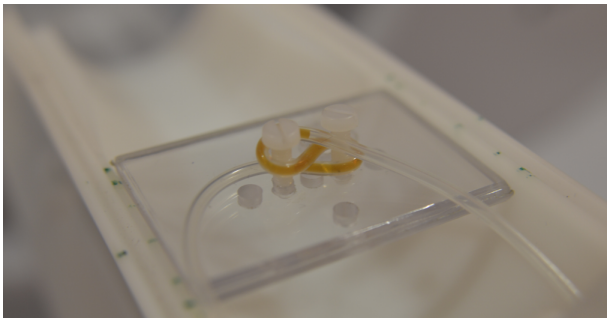

Figure 2: Eight-shaped hosepipe phantom with an inner diameter of 1 mm of a silicon tube and a 41.6 μL bolus of the MPI tracer.

In contrast to the nominal distribution of the MNP, we find a blurring of the MNP distribution in the x-y-plane of the reconstruction, with some MNP signal located outside of the limits of the tube (with a diameter of 1 mm). From the image, we estimate a two times bigger cross-section of about 2 mm. This reflects the resolution limit in x- and y- direction related to the gradient of 1.25 T/m. In z-direction (see Fig. 5), we estimate a cross-section of about 1 mm related to the gradient $G_z = 2.5$ T/m. Following the estimation of the resolution in [8] leads us to a size of the FFP of $2 \times 2 \times 1$ mm^3. However, we have not found remarkable differences for a SF with a reference sample size of $2 \times 2 \times 1$ mm^3 and one with $2 \times 2 \times 2$ mm^3, except the doubling of the SF amplitudes due to the bigger reference sample. That means we receive by the applied FFP volume the change of magnetization in the whole $2 \times 2 \times 2$ mm^3 reference sample. Therefore, we conclude that the FFP volume is bigger than the resolution. Using that, we can apply lower concentrated reference samples for acquiring the SF. That is important because the dynamic magnetic behavior of many tracers is changed at

high concentrations [5]. Thus, for quantitative MPI, reference samples of concentrations below 0.2 mol/L should be used.

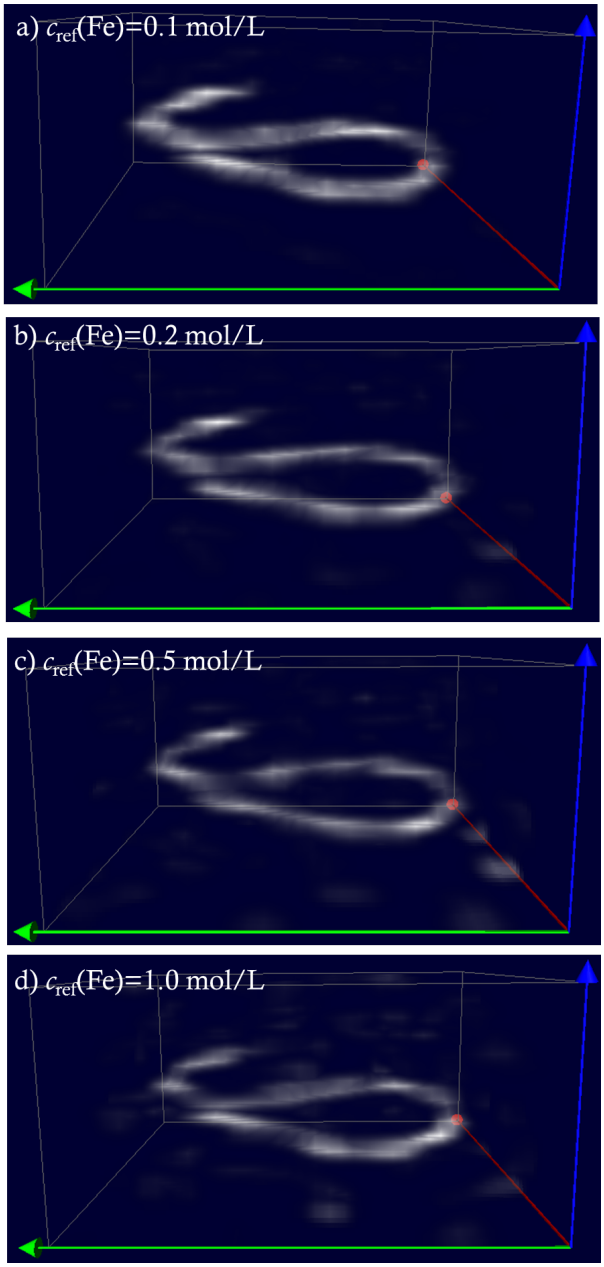

Figure 3: Side view of the reconstructed MPI images of the tracer bolus in the eight shaped phantom employing SF acquired with references at different (increasing) iron concentrations c_{ref}(Fe) = 0.1 mol/L (a), 0.2 mol/L (b), 0.5 mol/L (c), and 1 mol/L (d).

For a more detailed analysis, we defined a region of interest (ROI) in a particular voxel layer (layer 7 of 16 in z-direction, see Fig. 4, yellow rectangle), this produced a cross section in the middle of the silicon pipe phantom. For all four reconstructions, we determined the maximum and mean of the reconstructed intensity values in

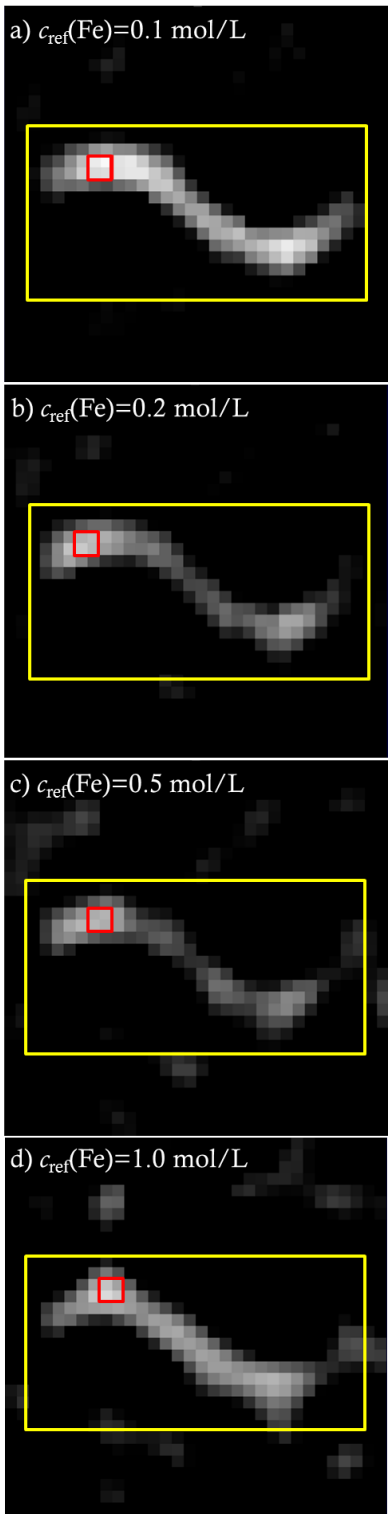

Figure 4: Selected ROI (yellow) to determine maximum and mean values of the four reconstructed images and selected group of 4 voxel (red) for c(Fe) calculation in layer 7 of FOV in z-direction (x-y-plane) using SF acquired with reference samples at different iron concentrations c_{ref}(Fe) = 0.1 mol/L (a), 0.2 mol/L (b), 0.5 mol/L (c), and 1 mol/L (d).

10.18416/ijmpi.2017.1706002

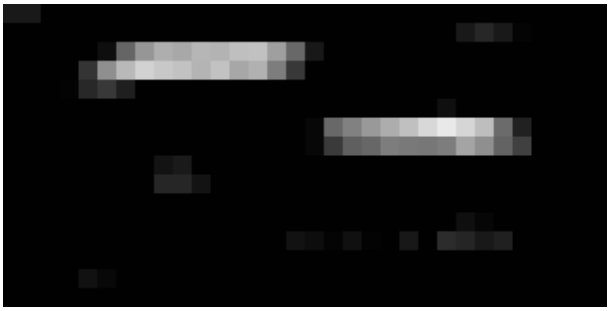

Figure 5: Side view in x-direction (y-z-plane) slice 12 of 32.

the selected ROI (yellow rectangle).

In Fig. 6 both values are plotted as a function of the inverse of the concentration used for SF acquisition, showing a clear linear relation. The straight lines in Fig. 6 display the linear regression to determine the slopes of mean and maximum as a function of $c_{\text{ref}}(\text{Fe})^{-1}$.

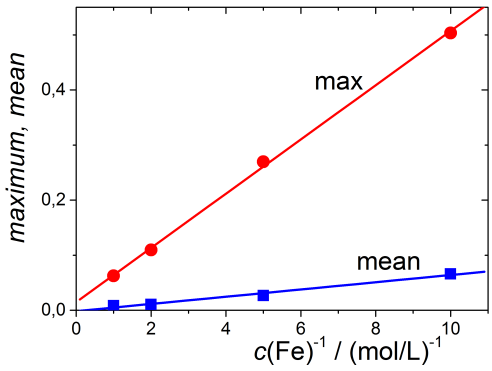

Figure 6: Maximum and Mean values within the ROI as a function of the inverse of the reference concentration $c_{\text{ref}}(\text{Fe})^{-1}$ used in SF acquisition.

The reconstructed image values (voxel intensity values) are scaled with the inverse of the concentration of the SF reference, as shown in Fig. 6. This implies that the recorded SF is not normalized to the concentration of the reference sample c_{ref}. Thus, the concentration of the reference sample employed for SF acquisition is linearly encoded in the system matrix $\bar{\boldsymbol{S}}$, i.e. doubling the concentration of the SF reference sample (keeping the same volume) doubles the detected signals of SF. By inverting $\bar{\boldsymbol{S}}$ for the solution of Eq. (6), we get a factor $c_{\text{ref}}(\text{Fe})^{-1}$ for all voxel values in our reconstruction.

$$m_{\text{Fe}}(\text{voxel}) = \frac{m_{\text{Fe,total}}}{c_{\text{ref,total}} \sum_{\text{voxel,total}} I_{\text{voxel}}} c_{\text{ref}} I_{\text{voxel}} \qquad (8)$$

To obtain a quantitative reconstruction we applied Eq. (8) using the SF with $c_{\text{ref}}(\text{Fe}) = 0.1$ mol/L, where we summed up the intensity values I_{voxel} of all voxels in the ROI (see Fig. 4) in the layers 3 to 11 and multiplied this sum by $c_{\text{ref}}(\text{Fe})$ to remove the concentration dependence of the SF. Then, by multiplying each voxel intensity I_{voxel} by the ratio of total amount of iron $m_{\text{Fe,total}} = 464.6\,\mu\text{g}$ and (concentration independent) total intensity value sum we obtained the iron content of each voxel. Tab. 1 shows the concentration c_{voxel} based on the iron content, and related to the voxel size (0.6875 mm^3).

Table 1: Iron content m_{Fe} and concentration c_{voxel} determined in the selected group of four voxels (red square, Fig. 4) from each of the four reconstructions using different SF reference samples with different iron concentrations.

$\boldsymbol{c_{\text{ref}}}$ in mol/L	**0.1**	**0.2**	**0.5**	**1.0**
Iron/voxel in μg	1.66	1.79	1.89	1.98
$\boldsymbol{c_{\text{voxel}}}$ in mol/L	0.091	0.099	0.10	0.11

Contrary to the nominal tracer concentration $c\,(\text{Fe}) = 0.2$ mol/L used in the pipe-phantom, this procedure resulted in a reconstructed concentration of about 0.1 mol/L in the voxel.

We trace this discrepancy back to the extension of reconstructed volume as a consequence of the lower resolution in x- and y-direction. The sharply limited cross section of the 1 mm pipe is found to be distributed over more than two voxels with an edge length of 0.6875 mm in the x-y-plane (see Fig. 4). It can be suppressed by a better resolution in x and y. Nevertheless, we see no way in general to discriminate between blurring and a real broader distributed MNP accumulation.

The concentration dependence of the SFs can also be found directly in the values of the frequency components in the modes of the SFs. In Fig. 7 a) section of the two SFs acquired at lowest and highest reference concentration, $c_{\text{ref}}(\text{Fe}) = 0.1$ mol/L and 1.0 mol/L, are displayed for the frequency mode $2f_x + 2f_y + 0f_z = 101.1$ kHz. By color and distribution these maps look very similar, but their absolute values (scaled grey values) differ by a factor of ten, corresponding to the ratio of concentrations. Of course we can find the concentration ratio even in the SNR values [7] for this mode with 8819.3 for $c_{\text{ref}}(\text{Fe}) = 1.0$ mol/L and 892.5 for $c_{\text{ref}}(\text{Fe}) = 0.1$ mol/L as a result of the higher concentration. In contrast to the absolute values in the voxels, this will be unchanged if we normalize the SF measurement following Eq. (7).

Previously, we observed that in Resovist spectra the higher harmonics decrease faster at increased concentrations [5]. For the precursor of Resovist, Ferucarbotran, we could confirm this behavior in a reduced form in SF modes at higher frequencies. As displayed in Fig. 8 for mode $6f_x + 6f_y + 6f_z$, at $f = 454.824$ kHz we obtained a slightly reduced factor of about 8.5. In contrast to Resovist, we could not discover changes in the phase, or in the distribution pattern of Ferucarbotran (see Fig. 7 and Fig. 8). In this respect, we found a change in the

magnetization behavior of Ferucarbotran, however less pronounced than observed in Resovist [5] and the dynamic magnetic behavior is nearly constant. However, we have to apply a reference sample at a concentration $c_{\text{ref}}(\text{Fe}) \leq 0.2\,\text{mol/L}$ for many other tracers.

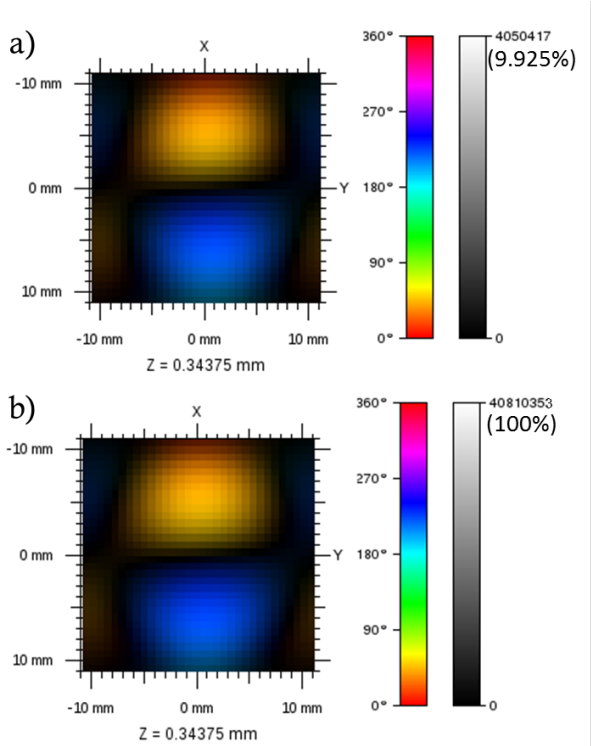

Figure 7: Graphical SF representations (x-y-plane at $z = 0.344\,\text{mm}$) using the SFView software [7] of mode $= 2f_x + 2f_y + 0f_z$, recorded with references at $c_{\text{ref}}(\text{Fe}) = 0.1\,\text{mol/L}$ (a) and $c_{\text{ref}}(\text{Fe}) = 1\,\text{mol/L}$ (b).

IV. Conclusions

We analyzed the influence of the tracer concentration of the reference sample used for SF acquisition on the reconstructed MPI images of a phantom. We found a linear relation between SF reference sample concentration and reconstructed image intensity values. Based on this we have calculated the iron quantity in each voxel of the reconstruction. Over a wide range of SF concentrations, we have obtained reconstructed concentrations of the phantom, which are consistent within a margin of ±10 %. We attribute the slightly increased iron concentration for the SF measured with higher concentrated reference sample to the increased noise sensitivity in the reconstruction. In order to improve the efficiency of the process in the future, we will implement the normalization by Eq. (7) of the SF used in the reconstruction. Considering that the total tracer amount in the blurred reconstructed image is distributed over an increased volume, we find that

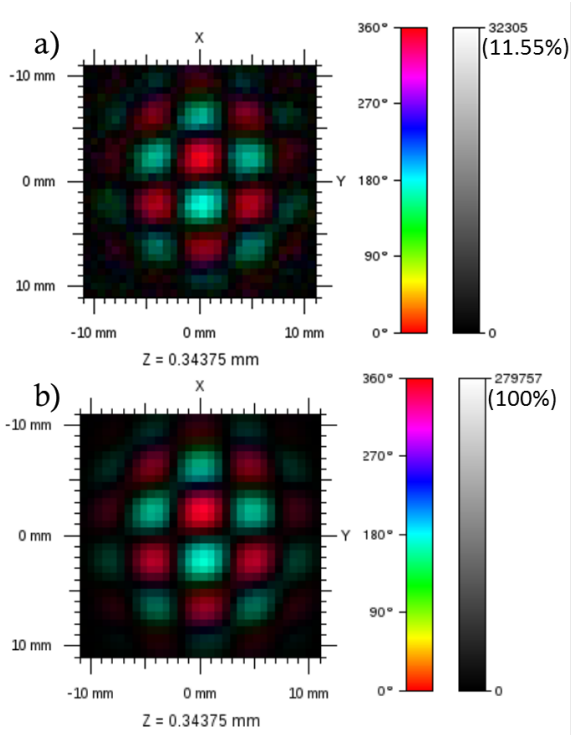

Figure 8: Graphical SF representations (x-y-plane at $z = 0.344\,\text{mm}$) using the SFView software [7] of mode $= 6f_x + 6f_y + 6f_z$, recorded with references at $c_{\text{ref}}(\text{Fe}) = 0.1\,\text{mol/L}$ (a) and $c_{\text{ref}}(\text{Fe}) = 1\,\text{mol/L}$ (b).

our results to be in agreement with the real tracer concentration. Our experimental study demonstrates that MPI can provide quantitative information on the spatial distribution of magnetic nanoparticles.

Acknowledgements

This work was supported by the DFG research program (quantMPI, grant TR408/9-1).

References

[1] J. Haegele, S. Vaalma, N. Panagiotopoulos, J. Barkhausen, F. M. Vogt, J. Borgert, and J. Rahmer. Multi-color magnetic particle imaging for cardiovascular interventions. *Phys. Med. Biol.*, 61(16):N415–N426, 2016. doi:10.1088/0031-9155/61/16/N415.

[2] J. Franke, U. Heinen, H. Lehr, A. Weber, F. Jaspard, W. Ruhm, M. Heidenreich, and V. Schulz. System Characterization of a Highly Integrated Preclinical Hybrid MPI-MRI Scanner. *IEEE Trans. Med. Imag.*, 35(9):1993–2004, 2016. doi:10.1109/TMI.2016.2542041.

[3] K. Lu, P. W. Goodwill, E. U. Saritas, B. Zheng, and S. M. Conolly. Linearity and Shift Invariance for Quantitative Magnetic Particle Imaging. *IEEE Trans. Med. Imag.*, 32(9):1565–1575, 2013. doi:10.1109/TMI.2013.2257177.

[4] J. Rahmer, J. Weizenecker, B. Gleich, and J. Borgert. Signal encoding in magnetic particle imaging: properties of the system function. *BMC Medical Imaging*, 9(4), 2009. doi:10.1186/1471-2342-9-4.

[5] N. Löwa, P. Radon, O. Kosch, and F. Wiekhorst. Concentration Dependent MPI Tracer Performance. *Intern. J. Magnetic Particle Imaging*, 2(1):1601001, 2016. doi:10.18416/ijmpi.2016.1601001.

[6] P. C. Hansen. *Discrete inverse Problems, Insight and Algorithms*. SIAM, Philadelphia, PA, 2010. doi:10.1137/1.9780898718836.

[7] SFView - A versatile MPI system function viewer, 2017. URL http://it.hs-pforzheim.de/personen/heinen/software/sfview.html.

[8] J. Borgert, J. D. Schmidt, I. Schmale, J. Rahmer, C. Bontus, B. Gleich, B. David, R. Eckart, O. Woywode, J. Weizenecker, J. Schnorr, M. Taupitz, J. Haegele, F. M. Vogt, and J. Barkhausen. Fundamentals and applications of magnetic particle imaging. *J. Cardiovasc. Comput. Tomogr.*, 6(3):149–153, 2012. doi:10.1016/j.jcct.2012.04.007.

